HHS Public Access

Author manuscript

Nat Struct Mol Biol. Author manuscript; available in PMC 2019 December 24.

Published in final edited form as:

Nat Struct Mol Biol. 2019 July ; 26(7): 583–591. doi:10.1038/s41594-019-0242-x.

Structural basis of tubulin detyrosination by vasohibins

Faxiang Li[1,2], **Yingjie Hu**[1,2], **Shutao Qi**[1,2], **Xuelian Luo**[1,3], and **Hongtao Yu**[1,2]

[1]Department of Pharmacology, University of Texas Southwestern Medical Center, Dallas, Texas, USA

[2]Howard Hughes Medical Institute, University of Texas Southwestern Medical Center, Dallas, Texas, USA

[3]Department of Biophysics, University of Texas Southwestern Medical Center, Dallas, Texas, USA

Abstract

Microtubules are regulated by posttranslational modifications (PTMs) of tubulin. The ligation and cleavage of the C-terminal tyrosine of α tubulin impact microtubule functions during mitosis, cardiomyocyte contraction, and neuronal processes. Tubulin tyrosination and detyrosination are mediated by tubulin tyrosine ligase (TTL) and the recently discovered tubulin detyrosinases, vasohibin 1 and 2 (VASH1 and VASH2) bound to the small vasohibin-binding protein (SVBP). Here, we report the crystal structures of human VASH1–SVBP alone, in complex with a tyrosine-derived covalent inhibitor, and bound to the natural product parthenolide. The structures and subsequent mutagenesis analyses explain the requirement for SVBP during tubulin detyrosination, and reveal the basis for the recognition of the C-terminal tyrosine and the acidic α tubulin tail by VASH1. The VASH1–SVBP–parthenolide structure provides a framework for designing more effective chemical inhibitors of vasohibins, which can be valuable for dissecting their biological functions and may have therapeutic potential.

Introduction

As an integral component of the cytoskeleton of eukaryotic cells, microtubules maintain cell shape and polarity, provide tracks for motor proteins to move cargos, and power chromosome movement during mitosis, among other functions[1]. Microtubules are polar polymers formed by α–β tubulin heterodimers, with a highly dynamic plus end and a less dynamic minus end. Tubulin heterodimers can be added to or rapidly lost from the plus end, leading to the growth or catastrophe of microtubules, a phenomenon termed dynamic instability[2,3]. Microtubule dynamics and functions are influenced by diverse microtubule-

Corresponding authors: Xuelian Luo (Xuelian.Luo@utsouthwestern.edu) and Hongtao Yu (Hongtao.Yu@utsouthwestern.edu).

Author contributions

F.L. performed protein purification, crystallization, structure determination, and functional studies *in vitro* and in human cells and wrote the initial draft of the paper. Y.H. and S.Q. performed the immunofluorescence assays in human cells. X.L. assisted in structure refinement, analyzed data, and supervised the research. H.Y. analyzed data, supervised the research, and edited the manuscript.

Competing interests

The authors declare no competing interests.

associated proteins (MAPs) and molecular motors[4]. The binding of MAPs and motors to microtubules is in turn regulated by myriad posttranslational modifications (PTMs) of tubulin[5–8], such as the enzymatic cleavage and ligation of tyrosine at the C-terminus of α tubulin[9].

The detyrosination-tyrosination cycle at the C-terminus of α tubulin was discovered more than four decades ago[10–12]. The tubulin tysosine ligase (TTL) was also purified and characterized long ago[13]. Tyrosination occurs exclusively on free α–β tubulin heterodimers as the TTL-interacting surface on tubulin is partially buried in microtubules[14]. By contrast, detyrosination preferably occurs on microtubules[15]. As a result, long-lived, stable microtubules contain more detyrosinated tubulin whereas dynamic, newly formed microtubules or microtubule segments contain more tyrosinated tubulins[16]. Tubulin tyrosination regulates the interaction between microtubules and MAPs. For example, several MAPs, including CLIP-170 and p150^{Glued}, contain the CAP-Gly domain, which preferably binds to tyrosinated tubulin[17].

TTL$^{-/-}$ mice exhibit perinatal lethality and disorganized neuronal networks in the brain, establishing a physiological role of tubulin tyrosination in neuronal development[18]. Moreover, proper levels of microtubule detyrosination confer optimal stiffness and contractility to beating cardiomyocytes[19,20]. Finally, the plus-end-directed microtubule motor CENP-E travels more processively on detyrosinated microtubules[21], which are oriented towards the equator of the mitotic spindle. This mechanism is critical for CENP-E-dependent movement of pole-proximal chromosomes to the metaphase plate and for accurate chromosome segregation[21].

Despite the importance of the tubulin detyrosination-tyrosination cycle, the enzymes responsible for tubulin detyrosination were only discovered very recently. In 2017, two independent studies identified the vasohibins 1 and 2 (VASH1 and VASH2) bound to the small vasohibin-binding protein (SVBP) as carboxypeptidases capable of tubulin detyrosination[22,23]. Depletion or chemical inhibition of VASH1–SVBP and VASH2–SVBP in cultured neurons delays axon differentiation, indicating a role of tubulin detyrosination in neuron polarization[22]. Loss of function mutations of *SVBP* have been linked to intellectual disability and microcephaly syndromes in humans[24]. The mechanism by which vasohibins detyrosinate tubulin is not understood, however.

In this study, we report the crystal structures of human VASH1–SVBP alone and bound to a tyrosine-derived covalent inhibitor. Our structures reveal how SVBP stabilizes the active site of VASH1 to promote detyrosination and how VASH1 recognizes the C-terminal tyrosine. Structure-based mutagenesis further pinpoints the requirement of positively charged residues that line the substrate-binding cleft for catalysis, which might be involved in binding the negatively charged C-terminal α tubulin tail. Finally, we determine the structure of VASH1–SVBP bound to the natural product, parthenolide, which is a known inhibitor of tubulin detyrosination[25]. The VASH1–parthenolide structure provides a blueprint for the development of more potent, specific inhibitors of VASH1 and VASH2, which may have therapeutic values.

Results

Crystal structure of the VASH1–SVBP complex

The central region of vasohibins (VASH1 and VASH2) contains a transglutaminase-like cysteine protease domain (Fig. 1a). Ectopically expressed Myc-VASH1–SVBP catalyzed α-tubulin detyrosination in human cells and taxol treatment enhanced this detyrosination (Fig. 1b), confirming that VASH1–SVBP is indeed a functional tubulin detyrosinase with a preference for microtubules. We co-expressed the protease domain of human VASH1 (residues 52–310) and VASH2 (residues 42–314) with full-length SVBP in bacteria and purified the resulting VASH1–SVBP and VASH2–SVBP complexes (Fig. 1c). Recombinant VASH1–SVBP and VASH2–SVBP complexes catalyzed the detyrosination of recombinant human microtubules stabilized by the non-hydrolyzable GTP analog GMPCPP (Fig. 1d). VASH1–SVBP detyrosinated microtubules more efficiently than soluble α–β tubulin heterodimer (Fig. 1e). VASH1–SVBP and VASH2–SVBP also catalyzed the detyrosination of the C-terminal tail of human α-tubulin (CTα) fused to GST (Fig. 1f). As expected, mutation of the catalytic cysteine C169 of VASH1 abolished the activity of VASH1–SVBP towards microtubules and CTα (Fig. 1d,f). Thus, the recombinant VASH1–SVBP and VASH2–SVBP complexes are functional.

To understand the detyrosination mechanism of vasohibins, we determined the crystal structure of VASH1–SVBP to 2.1 Å resolution (Fig. 1e,f and Table 1). The protease domain of VASH1 consists of an N-terminal extension (NTE), a small helical N-lobe containing three helices and a large C-lobe with a mixed αβ fold. The active site lies at the interface between the N- and C-lobes. The central region of SVBP folds into a single long helix. VASH1 and SVBP form a simple 1:1 heterodimeric complex with an overall shape that resembles a ski lift. The long helix of SVBP forms the rail. The αA and αB helices of the NTE of VASH1 latch onto this rail. A proline-rich linker acts as the arm that connects this N-terminal latch to the globular protease domain, which forms the base of the lift chair.

A structural comparison search using the Dali server revealed that the protease domain of VASH1 has a fold similar to that of the Ca^{2+}-dependent transglutaminase-like cysteine protease LapG from bacterial pathogens (Supplementary Fig. 1a)[26]. Similar to VASH1, LapG consists of a helical N-lobe and a C-lobe with a seven-stranded β sheet. There are major structural differences between the two proteins, however (Supplementary Fig. 1b,c). First, the N-lobe of LapG has five α helices whereas the N-lobe of VASH1 has only three. The first two helices of VASH1 (αA and αB) form the NTE that wraps around SVBP. Second, the C-lobe of LapG contains only one long helix (αF), as opposed to two long helices (αF and αG) in the C-lobe of VASH1. Moreover, the C-terminal helix αF of LapG packs against its N-lobe whereas the C-terminal helix of VASH1 does not contact the N-lobe (Supplementary Fig. 1b,c). Finally, the transglutaminase-like cysteine protease superfamily of enzymes, including LapG, has the canonical Cys-His-Asp (or Cys-His-Glu) catalytic triad[27]. In contrast, VASH1 does not have the Asp or Glu residue in the triad. Instead, it has a serine residue (S221) in place of the Asp or Glu (Fig. 1a and Supplementary Fig. 1d). VASH1 has been proposed to have a non-canonical Cys-His-Ser catalytic triad that consists of C169, H204, and S221[27]. Surprisingly, S221 is too far away from H204 and cannot form

a hydrogen bond with H204 (Supplementary Fig. 1d). The main chain carbonyl group of L226 does, however, form a hydrogen bond with the imidazole group of H204. C169 resides in the N-lobe while H204 and S221 are located in the C-lobe. All three residues are conserved across species (Supplementary Fig. 2a).

Molecular interactions between VASH1 and SVBP

SVBP forms a single α helix, which is encircled by the NTE and the N-lobe of VASH1 (Fig. 1e,f). The midsection of the SVBP helix (residues 31–50) forms extensive hydrophobic and electrostatic interactions with residues in αA, αB, the loop preceding αA, the αB–αC loop, the αC–αD loop, and the αD–αE loop (Fig. 2a,b and Supplementary Fig. 2). In particular, SVBP I39 and Y40 pack against L67, W74, M77, I104, F141, L165, and P166 from VASH1. Likewise, A41, L42, V45, and M46 from SVBP form extensive hydrophobic interactions with W74, W78, V81, V91, and I95, which are located on αA and αB of VASH1. In addition, SVBP K32 makes favorable electrostatic interactions with E163 of VASH1, while SVBP E50 makes two salt bridges with R222 and H136 from VASH1. Most residues at the VASH1–SVBP interface are highly conserved (Supplementary Fig. 2).

Recombinant VASH1 formed inclusion bodies when expressed in bacteria in the absence of SVBP, indicating that SVBP is required for the proper folding and solubility of VASH1 in a heterologous system. VASH1 mutants that are deficient for SVBP binding are unlikely to be obtained as soluble proteins in bacteria. To validate the functional relevance of the VASH1–SVBP interface observed in our structure, we made several VASH1 and SVBP mutants that changed the hydrophobic residues at their interface to charged ones, transfected these plasmids into HeLa cells (which had low endogenous levels of tubulin detyrosination), and evaluated their ability to detyrosinate α tubulin. Single point mutations of VASH1 (M77R, V81R and F141R) or SVBP (I39E and L42E) did not dramatically reduce the detyrosination activity of the ectopically expressed VASH1–SVBP (Fig. 2c,d).

One possibility is that these single point mutations could not disrupt the VASH1–SVBP interaction, owing to the extensive interface between the two proteins. We thus constructed double and triple mutants targeting multiple residues simultaneously. When co-expressed with wild-type (WT) SVBP, the detyrosination activities of VASH1 M77R/F141R, V81R/F141R, and M77R/V81R/F141R (3R) were greatly reduced, as compared to WT VASH1 (Fig. 2c,d). Likewise, the SVBP I39E/L42E double mutant was much less efficient than the WT SVBP in supporting VASH1-dependent tubulin detyrosination. These results indicate that the VASH1–SVBP interface observed in the crystal structure is critical for the catalytic activity of VASH1.

The protein levels of these functionally deficient VASH1 and SVBP mutants were not substantially lower than those of the WT or functionally active mutants (Fig. 2c). Thus, perturbing the VASH1–SVBP interface does not necessarily destabilize the VASH1 protein. Because the αC–αD and the αD–αE loops that contact SVBP are in close spatial proximity to the catalytic triad (Fig. 2c,d and Supplementary Fig. 2a), SVBP might promote tubulin detyrosination through maintaining the structural integrity of the active site of VASH1.

Recognition of the C-terminal tyrosine by VASH1–SVBP

To understand the substrate specificity of VASH1, we crystalized the catalytically inactive VASH1 C169S–SVBP complex in the presence of 5 molar equivalent of α tubulin C-terminal peptide. Unfortunately, none of the structures determined using these crystals contained clear electron density for the tubulin peptide. The interaction between VASH1 and peptide substrates was thus too transient to be captured by crystallization. We thus synthesized the epoxide-coupled tyrosine (epoY) compound, which had been shown to be a covalent inhibitor of VASH1 (Fig. 3a)[22]. EpoY is thought to bind to the substrate-binding site of VASH1 through the tyrosine moiety and then become covalently linked to the catalytic cysteine through the epoxide group, thereby inhibiting VASH1. Consistent with previous results[22], epoY inhibited the detyrosination of microtubules by VASH1–SVBP in a dose-dependent manner (Supplementary Fig. 3a).

We obtained crystals of VASH1–SVBP bound to epoY that diffracted to 1.83 Å resolution and determined the structure of this complex using molecular replacement. There was clear electron density for epoY, which was indeed covalently linked to C169 at the active site (Fig. 3b,c). Superimposition of the apo-VASH1 and epoY-bound VASH1 shows that epoY binding does not induce substantial conformational changes of the active site (Fig. 3d). EpoY fits snugly in the substrate-binding cleft formed by the N- and C-lobes of VASH1 (Fig. 3c and Supplementary Fig. 3b). The aromatic ring of the tyrosine from epoY forms cation-π interactions with R222 (Fig. 3e). The backbone carboxyl group of the tyrosine forms hydrogen bonds with the hydroxyl group of S221 and the main chain amide group of R222, and develops favorable electrostatic interactions with the side chain of R222 (Supplementary Fig. 3c). These interactions enable the recognition of the C-terminal tyrosine by VASH1.

The Asp or Glu in the canonical Cys-His-Asp or Cys-His-Glu catalytic triad found in other transglutaminase-like cysteine proteases positions the His for the deprotonation of the active-site Cys and the formation of a thiolate–imidazolium ion pair between Cys and His residues[27]. Vasohibins have been proposed to have a non-canonical Cys-His-Ser catalytic triad (Fig. 1a), but the serine in this putative triad is too far away to form a hydrogen bond with the histidine (Supplementary Fig. 1d). Instead, S221 in the proposed catalytic triad of VASH1 is involved in the recognition of the C-terminal carboxyl group (Fig. 3e and Supplementary Fig. 3c).

To clarify the roles of the catalytic residues, we quantitatively measured the catalytic activities of the VASH1 S221A and H204A mutants (Table 2). (The C169S mutant does not have enough residual activity for us to measure its activity.) The H204A mutation greatly reduced the k_{cat} of VASH1 without affecting the K_m, consistent with it being a part of the catalytic triad. By contrast, the S221A mutation only reduces the k_{cat} 3-fold, but greatly increases the K_m. These data are consistent with S221 playing a critical role in substrate binding through its interactions with the C-terminal carboxyl group. S221 is unlikely to be a part of the catalytic triad. Instead, H204 forms a hydrogen bond with the main chain carbonyl of L226 (Supplementary Fig. 1c). L226 and its interacting residues A246 and Y247 are conserved in VASH1 and VASH2 proteins from different species (Supplementary Fig. 2a). These conserved interactions position the L226 carbonyl group for hydrogen bonding

with H204. Thus, the main chain carbonyl group of L226 in VASH1 serves the purpose of the side chain carboxyl group of the aspartate in the canonical catalytic triad.

The hydroxyl group of Y134 forms a hydrogen bond with the backbone carbonyl group of the scissile bond (Fig. 3e and Supplementary Fig. 3c). This interaction likely stabilizes the oxyanion of the tetrahedral intermediate formed by C169 and the substrate during catalysis. In addition, K168 occupies a position that can potentially allow it to interact with the acidic side chain of the penultimate residue in the authentic tubulin substrate. Consistent with these structural observations, the Y134A and K168E mutations greatly reduced the catalytic efficiency of VASH1–SVBP in vitro (Table 2). Finally, L170 and I205 interact with the ethyl ester moiety of epoY. These two residues may interact with the peptide backbone of the tubulin C-terminal tail.

To further ascertain the functional requirement of key residues of VASH1 that directly contacted epoY, we tested whether mutations of these residues affected tubulin detyrosination in HeLa cells. When co-expressed with SVBP, wild-type (WT) VASH1 produced detyrosinated tubulin in these cells, as indicated by immunoblotting and immunofluorescence (Fig. 3f,g and Supplementary Fig. 3d). By contrast, mutations of the catalytic residues, Y134 (which stabilizes the oxyanion intermediate), or R222 (which recognizes the C-terminal tyrosine on substrates) greatly reduced tubulin detyrosination by VASH1. These results validate the functional relevance of the substrate-binding mode observed in the VASH1–SVBP–epoY structure.

Role of basic residues lining the substrate-binding cleft

All human α tubulin isoforms, except TUBA4A, encode a C-terminal tyrosine or phenylalanine, and can be cleaved by vasohibin–SVBP complexes. The C-terminal tails of all α tubulin isoforms are very acidic and contain multiple glutamates (Supplementary Fig. 4a). Several conserved basic residues line the substrate-binding cleft between the N- and C-lobes of VASH1 (Fig. 4a). Electrostatic surface potential maps reveal that this substrate-binding cleft is indeed highly positively charged (Fig. 4b). We suspect that these basic residues are involved in the recognition of the acidic C-terminal tail of α tubulin.

To test this hypothesis, we mutated these conserved basic residues to glutamates individually or in combination and tested the ability of these single or double mutants to support tubulin detyrosination in HeLa cells using both immunoblotting and immunofluorescence assays (Fig. 4c,d and Supplementary Fig. 4b,c). Among the mutants tested, the VASH1 K146E and K168E single mutants were almost completely defective whereas R203E was partially defective. The K146E and K168E mutations also greatly reduced the catalytic efficiency of VASH1 in vitro (Table 2). Thus, these three basic residues clearly contribute to tubulin detyrosination, possibly through interacting with the glutamates in the C-terminal tail of α tubulin. Even though the K258E single mutant was functional, the R203E/K258E double mutant was more defective than the R203E single mutant, suggesting a small contribution of K258 in substrate recognition. Mutations of VASH1 K194, K256, and K276 had little effect on tubulin detyrosination. These residues are located farther away from the substrate-binding cleft (Fig. 4a), and do not appear to be involved in substrate binding.

Sequence alignment reveals that the protease domains of human VASH1 and VASH2 share 52% identity (Supplementary Fig. 5a). In particular, the catalytic triad, the serine that recognizes the C-terminal carboxyl group, and the basic residues lining the substrate-binding cleft are conserved between the two proteins. Mutations of these residues in VASH2 greatly reduced the tubulin detyrosination activities of VASH2 in HeLa cells (Supplementary Fig. 5b), suggesting that the mode of substrate recognition is conserved between VASH1 and VASH2. We note that the VASH2 S210A mutant and several other mutants exhibited detectable residual activities. Mutants targeting VASH1 catalytic residues also exhibited residual activities in vitro, which allowed us to measure their k_{cat} and K_m values. Thus, single point mutations of these active site residues do not completely abolish the catalytic activities of this class of enzymes.

Mechanism of VASH1 inhibition by parthenolide

Parthenolide is a natural product isolated from the medicinal plant feverfew (*Tanacetum parthenium*), which has been traditionally used to treat fevers, migraines, rheumatoid arthritis, and other illnesses. Parthenolide has a variety of reported biological activities, including modulation of the NF-κB-mediated inflammatory responses[28], induction of apoptosis[29], inhibition of mammalian thioredoxin reductase[30], and inhibition of microtubule detyrosination[25]. It is a sesquiterpene lactone and contains two reactive groups: the epoxide and α-methylene (Fig. 5a). Despite the multiple proposed functions, the mechanisms by which parthenolide inhibits any of its putative targets are unknown. In particular, it is unclear whether the epoxide or the α-methylene is the reactive group.

We first confirmed that parthenolide at high concentrations indeed partially inhibited tubulin detyrosination by VASH1–SVBP in HeLa cells (Fig. 5b). To further define the mechanism of inhibition, we determined the crystal structure of VASH1–SVBP in complex with parthenolide to a resolution of 2.0 Å (Fig. 5c). The electron density clearly shows that parthenolide is bound to the active-site cysteine of VASH1 (Fig. 5d). The electron density of certain parthenolide atoms, particularly that of C9, is weaker than that of the rest of the molecule, indicative of conformational disorder in this portion of parthenolide. Binding of parthenolide does not induce substantial conformational changes of the active site of VASH1 (Supplementary Fig. 6)

Parthenolide is covalently linked to the thiol of C169 of VASH1 through C13 (Fig. 5a,d). Thus, the thiol group of C169 reacts with the α-methylene of parthenolide through a Michael addition reaction, not with the epoxide of parthenolide. The reaction occurs in an enantioselective fashion, yielding only one of the two diastereomers (Fig. 5a). This covalent modification of C169 inactivates the protease activity of VASH1. Aside from the covalent linkage to C169, parthenolide makes hydrophobic interactions with surrounding residues, including Y134, K168, F202, H204, R222, and L226 (Fig. 5e). The oxygen of the epoxide in parthenolide forms a hydrogen bond with the hydroxyl group of S221. The carbonyl group from the lactone of parthenolide forms a hydrogen bond with the main chain amide group of C169. These non-covalent interactions position parthenolide optimally for nucleophilic attack by the catalytic cysteine of VASH1 in an enantioselective way.

Discussion

Our structures and mutagenesis analyses indicate that vasohibins recognize the C-terminal tyrosine of α tubulin through a serine residue (S221 in VASH1 and S210 in VASH2) and a nearby arginine (R222 in VASH1 and R211 in VASH2), and likely interact with acidic residues in the C-terminal tail of α tubulin through conserved basic residues lining the substrate-binding cleft (Fig. 5f). These observations explain the substrate specificity of vasohibins in cleaving the last tyrosine of α tubulin.

Shortly after the discovery of the activity of tubulin carboxypeptidases, it has become known that these enzymes prefer to cleave the tyrosine of α tubulin in microtubules, as compared to soluble α–β tubulin heterodimers[15]. Indeed, vasohibin–SVBP complexes display this preference in human cells, as the microtubule-stabilizing drug Taxol greatly enhances VASH1–SVBP-dependent tubulin detyrosination[23] (Fig. 1b). Our structure does not yet explain the preference of VASH1 and VASH2 towards microtubules. Further structural and biophysical studies of VASH1–SVBP and VASH2–SVBP in complex with microtubules are needed to elucidate the basis of this preference. It is possible that VASH1–SVBP and VASH2–SVBP make additional uncharacterized contacts with the microtubule lattice (Fig. 5f).

The tubulin tails are combinatorially modified by multiple posttranslational modifications to generate a tubulin code that regulates the binding of MAPs and microtubule dynamics and function[6]. In addition to the detyrosination-tyrosination cycle, the C-terminal tail of α tubulin can be modified by polyglutamation and polyglycation. It will be interesting to test whether these other modifications can regulate tubulin detyrosination by VASH1–SVBP and VASH2–SVBP, and vice versa.

The levels of tubulin tyrosination are dynamically controlled by opposing activities of TTLs and detyrosinases, including vasohibins. Upon microtubule depolymerization, soluble detyrosinated α–β tubulin can be re-tyrosinated by TTLs. Alterations of tubulin tyrosination levels caused by the genetic ablation of vasohibins can be blunted by the compensatory reduction of TTL activities. Thus, functional analysis of vasohibins in vivo can benefit from the availability of specific chemical inhibitors that can acutely inhibit these enzymes. Our structure of VASH1–SVBP bound to parthenolide provides an important starting point for designing more potent inhibitors of VASH1 and VASH2, which can be used as tool compounds to probe the functions of vasohibins and the acute effects of their inhibition in human cells and in animal models.

Methods

Antibodies and chemicals

The following antibodies against human proteins were used for immunoblotting and immunofluorescence: anti-Myc (Roche, Basel, Switzerland, 11667203001), anti-α tubulin (Sigma-Aldrich, T6199–100UL), anti-detyrosinated tubulin (EMD Millipore, AB3201), and anti-GST (Sigma-Aldrich, SAB4200237–200UL). Parthenolide (Sigma-Aldrich, P0667–25MG), Taxol (Cytoskeleton, TXD01), and GMPCPP (Jena bioscience, NC0641143) were

purchased from the indicated sources. The epoY inhibitor was synthesized by KareBay Biochem, Inc.

Protein expression and purification

The cDNA fragments encoding the catalytic domain of human VASH1 (residues 52–310) or VASH2 (residues 42–314) were amplified by PCR and cloned into the pRSF-32M vector (a modified version of the pRSF-Duet vector that introduces N-terminal thioredoxin and His_6 tags before the first multiple cloning site) for recombinant protein expression. The cDNAs encoding full-length human SVBP or its VASH1- and VASH2-binding region (residues 25–51) were cloned into the pET-32M vector (a modified version of pET32a that introduces N-terminal thioredoxin and His_6 tags). Point mutants of VASH1 or SVBP were constructed with the Q5 site-directed mutagenesis kit (NEB, E0554) following the manufacturer's protocols and confirmed by DNA sequencing.

The plasmids encoding VASH1 (or VASH2) and SVBP were co-transformed into BL21 (DE3) *E. coli* competent cells, and the bacteria were cultured in the LB medium at 37°C. When the OD_{600} of the culture reached 0.8, protein expression was induced by the addition of 300 μM IPTG at 16°C. The culture was further incubated at 16°C overnight. For preparation of the selenomethionine (SeMet)-labeled protein, the cells were cultured in the M9 minimal medium at 37°C. SeMet (259960025, Acros Organics) was added to 50 mg l^{-1}, and Lys-Thr-Phe (100 mg l^{-1}) and Leu-Ile-Val (50 mg l^{-1}) were also added to inhibit the endogenous synthesis of Met. The temperature was reduced to 16°C when the OD_{600} of the culture reached 0.6, and then protein expression was induced by the addition of IPTG to a final concentration of 500 μM, followed by further incubation at 16°C overnight.

The collected cell pellets were resuspended in 5 volumes of the binding buffer (50 mM Tris-HCl, pH 7.9, 500 mM NaCl, 5 mM imidazole) and lysed by sonication on ice. The lysate was cleared by centrifugation at 35,000 g for 30 min. The supernatant was transferred into a new 50-ml centrifuge tube and mixed with Ni^{2+}-NTA agarose resin (Qiagen, 30230) that had been pre-equilibrated by the binding buffer. The mixture was incubated at 4°C for 1 hour with rotation. The target proteins were eluted from the Ni^{2+}-NTA agarose resin by the elution buffer (50 mM Tris-HCl, pH 7.9, 100 mM NaCl, 300 mM imidazole) after extensive washing with the wash buffer (50 mM Tris-HCl, pH 7.9, 500 mM NaCl, 30 mM imidazole). The 3C protease was added to the eluted proteins at 4°C overnight to cleave the N-terminal thioredoxin tag. The cleaved proteins were then purified with the Resource S cation exchange column to remove the cleaved tag and other impurities. Finally, the protein fractions were collected and concentrated, and further purified by the Superdex 200 10/300GL size exclusion column.

For the purification of the C-terminal tail of human TUBA1A (residues 441–452) fused to GST (GST-CTα), the cell pellets were resuspended in PBS and lysed by sonication on ice. The pre-equilibrated glutathione Sepharose 4B resin (GE Healthcare) was applied to the cleared supernatant. After extensive wash with PBS, the protein was eluted by the elution buffer (50 mM Tris-HCl, pH 7.5, 100 mM NaCl, 15 mM reduced L-Glutathione). The eluted protein was concentrated, and further purified with the Resource Q anion exchange column and the Superdex 200 10/300GL size exclusion column. The protein fractions were

collected, concentrated, and stored at −80°C for future use. A list of primers and proteins used in this study is provided in Supplementary Table 1.

Crystallography

The Se-Met-labeled $VASH1_{52–310}$–SVBP complex was concentrated to 20 mg ml^{-1} in the buffer containing 25 mM Tris-HCl, pH 7.5, 100 mM NaCl, and 1 mM DTT and used for crystallization. Crystals of the VASH1–SVBP complex were obtained with the sitting-drop vapor-diffusion method at 20°C after 1 week by mixing 0.3 μl complex protein with an equal volume of the reservoir solution containing 0.1 M sodium citrate tribasic dihydrate, pH 5.0, and 18% (w/v) PEG20000. Parthenolide (Sigma-Aldrich, P0667–25MG) was dissolved in DMSO to make a 250 mM stock solution. The parthenolide-bound protein complex was made by mixing the freshly purified $VASH1_{52–310}$–SVBP complex with the parthenolide solution at the molar ratio of 1:10 and incubating the mixture at 4°C overnight. Crystals of the VASH1–SVBP–parthenolide complex were obtained with the sitting-drop vapor-diffusion method at 20°C after 2 weeks by mixing 0.3 μl protein complex (15 mg ml^{-1}) with an equal volume of the reservoir solution containing 0.2 M ammonium sulfate, 0.1 M Bis-tris, pH 5.5, and 25 % (w/v) PEG 3350. The epoY inhibitor was dissolved in the protein storage buffer to make a 10-mM stock solution. The freshly purified $VASH1_{52–310}$–$SVBP_{25–51}$ complex was mixed with the epoY inhibitor solution at the molar ratio of 1:5 and then incubated at 4°C for 4 hours before crystallization. Crystals of the VASH1–SVBP–epoY complex were obtained with the sitting-drop vapor-diffusion method at 20°C after 1 week by mixing 0.3 μl protein complex (15 mg ml^{-1}) with an equal volume of the reservoir solution containing 5% (v/v) Tacsimate™, 0.1 M HEPES, pH 7.0, and 10% (w/v) polyethylene glycol monomethyl ether 5,000. Glycerol (15%; v/v) was added to all crystals as the cryo-protectant before diffraction experiments. High-resolution X-ray diffraction datasets were collected at 100 K at the Structural Biology Center (Beamline 19ID) at the Advanced Photon Source (APS). Diffraction data were reduced and scaled using the HKL3000 software package[31].

The phase of the SeMet-labeled VASH1–SVBP dataset was determined by the single-wavelength anomalous diffraction (SAD) method. A partial structural model was built with the program AutoSol in the Phenix software[32]. The structure model was further built manually using the program Coot[33,34], and then refined with Phenix. The phases of the parthenolide- and epoY-bound VASH1–SVBP datasets were determined by molecular replacement with Phaser in Phenix[35], using the apo-VASH1–SVBP structure as the search model. The models of inhibitor-bound structures were built and refined as described above for the VASH1–SVBP structure. The qualities of the final models were verified with MolProbity[36]. Data collection and refinement statistics are summarized in Table 1.

In vitro detyrosination assays

For *in vitro* detyrosination assays with GST-CTα (α tubulin C-terminal tail) as the substrate, 100 nM of VASH1–SVBP or VASH2–SVBP wild-type or mutants were incubated with 500 nM GST-CTα in the buffer containing 25 mM Tris, pH 7.5, 100 mM NaCl, 1 mM DTT. The mixture was incubated at 37°C for 1 hour. The samples were mixed with the SDS loading buffer, boiled and subjected to immunoblotting. For *in vitro* detyrosination assays of

microtubules, recombinant human TUBA1B–TUBB3 heterodimer[37] (kindly provided by Drs. Xuecheng Ye and Luke Rice; UT Southwestern Medical Center) was thawed on ice and then filtered through 0.1 μm centrifugal filters (EMD Millipore, UFC30VV00) at 4°C to remove protein aggregates. The filtered protein was diluted to the final concentration of 10 μM in the BRB80 buffer (80 mM PIPES, pH 6.9, 1 mM $MgCl_2$, and 1 mM EGTA) with or without 10 mM GMPCPP. The GMPCPP-stabilized microtubules were polymerized at 37°C for 1 hour. The polymerized and non-polymerized α–β tubulin proteins were diluted to 0.5 μM with warmed BRB80 buffer. VASH1–SVBP or VASH2–SVBP wild-type or mutants (100 nM) were then incubated with 200 nM polymerized or non-polymerized α–β tubulin in the BRB80 buffer. The mixture was incubated in 37°C for the indicated times. The samples were mixed with the SDS loading buffer, boiled, and subjected to immunoblotting.

Enzymatic assays

Wild-type and mutant VASH1–SVBP proteins (50 nM) were incubated with varying concentrations of GST-CTα in the buffer containing 25 mM Tris, pH 7.5, 100 mM NaCl, 1 mM DTT. The reaction mixtures were incubated at room temperature for 2 min. The reactions were stopped by the addition of the SDS loading buffer. The samples were boiled and subjected to SDS-PAGE followed by quantitative immunoblotting. To determine the concentrations of detyrosinated tubulin product, we purified GST-CTα protein without the last tyrosine and loaded it onto the same gels as a standard for quantification. Three technical repeats were included for each reaction conditions. The initial velocities of the reactions were blotted against substrate concentrations with GraphPad Prism. The reaction curves were fitted to the standard Michaelis-Menten equation to determine the k_{cat} and K_m values.

Cell culture, transfection, and immunoblotting

HeLa Tet-On cells (Takara Bio USA, Inc., Mountain View, CA) were grown in DMEM (Invitrogen, Carlsbad, CA) supplemented with 10% fetal bovine serum (FBS) and 2 mM L-glutamine. The cell line has been validated to be of HeLa origin by STR profiling. We routinely check the cell line by DAPI staining to ensure that it is not contaminated by mycoplasma. All mammalian expression plasmids used in this study were derived from the modified pCS2 vector with N-terminal Myc_6 tags. Plasmid transfection was performed using the Lipofectamine™ 2000 Transfection Reagent (Thermo Fisher Scientific, 11668019) according to the manufacturer's protocols. Cells in each well of a 12-well plate were transfected with a total of 1 μg plasmids when the cell density reached 70% confluency. For analysis of the α tubulin detyrosination activity of vasohibins and SVBP mutants, the cells were washed once with PBS at 24 hours post-transfection and collected by directly resuspending them in the SDS loading buffer. The samples were boiled and subjected to immunoblotting with appropriate antibodies. The primary antibodies were used at a final concentration of 1 μg ml^{-1} diluted in the TBS buffer containing 0.1% Tween 20 and 5% milk. Anti-mouse IgG (H+L) (Dylight 680 conjugates) and anti-rabbit IgG (H+L) (Dylight 800 conjugates) (Cell Signaling, Danvers, MA) were used as secondary antibodies. The blots were scanned with an Odyssey Infrared Imaging System (LI-COR, Lincoln, NE).

Immunofluorescence

HeLa Tet-On cells were cultured and seeded in the chamber slides (Nunc Lab-Tek II CC2). Each well of the chamber slides was transfected with a total of 400 ng plasmids when cells reached 70% confluency. At 24 hours post-transfection, the cells were fixed with 4% paraformaldehyde for 15 min at room temperature. Cells on slides were permeabilized with PHEM buffer containing 0.2 Triton X-100 and blocked with PBS containing 3% BSA for 20 min. The fixed cells were incubated with the first primary antibody (anti-detyrosinated tubulin) diluted in PBS containing 0.2% Triton X-100 (PBST) and 3% BSA at 4°C overnight. After 3 washes with PBST for 5 min each, cells were incubated for 30 min at room temperature in the dark with the secondary antibody conjugated to Alexa Fluor® 488 (Thermo Fisher Scientific, A11008) diluted in PBST and 3% BSA. Cells were then washed 3 times with PBST for 5 min each and incubated with the anti-α tubulin antibody diluted in PBST and 3% BSA at 4°C overnight. After 3 washes with PBST for 5 min each, cells were incubated with the secondary antibody conjugated to Alexa Fluor® 568 (Thermo Fisher Scientific, A11004) diluted in PBST and 3% BSA for 30 min at room temperature in the dark. The cells were washed three times with PBST again and stained with 1 μg ml^{-1} DAPI in PBS for 2 min at room temperature. After the final wash with PBS, the cells were mounted using VECTASHIELD anti-fade mounting medium (Vector Laboratories), and the slides were sealed with nail polish. The cell images were captured with a 63X objective on a DeltaVision fluorescence microscope (GE Healthcare), deconvolved, and further processed with ImageJ.

Data availability

The coordinates and structure factors of the crystal structures of human VASH1–SVBP, VASH1–SVBP in complex with epoY, and VASH1–SVBP bound to parthenolide have been deposited into the Protein Data Bank with the accession codes 6OCF, 6OCG, and 6OCH, respectively. Source data for Figure 2d, 4c, Supplementary Figure 3d, and Table 2 are available in Supplementary Data Set 2. All other data are available from the corresponding authors upon request.

Supplementary Material

Refer to Web version on PubMed Central for supplementary material.

Acknowledgements

We thank Z. Chen and D. Tomchick for assistance with X-ray diffraction data collection and X. Ye and L. Rice for providing the recombinant human tubulin and for helpful discussions. Results shown in this report are derived from work performed at Argonne National Laboratory, Structural Biology Center at the Advanced Photon Source. Argonne is operated by UChicago Argonne, LLC, for the U.S. Department of Energy, Office of Biological and Environmental Research under contract DE-AC02-06CH11357. This study is supported by grants from the National Institutes of Health (GM107415 to X.L.), Cancer Prevention and Research Institute of Texas (RP160255 to X.L. and RP160667-P2 to H.Y.) and the Welch Foundation (I-1932 to X.L. and I-1441 to H.Y.). H.Y. is an Investigator with the Howard Hughes Medical Institute.

References

1. Dogterom M & Koenderink GH Actin-microtubule crosstalk in cell biology. Nat. Rev. Mol. Cell Biol 20, 38–54 (2019). [PubMed: 30323238]

2. Mitchison T & Kirschner M Dynamic instability of microtubule growth. Nature 312, 237–242 (1984). [PubMed: 6504138]
3. Desai A & Mitchison TJ Microtubule polymerization dynamics. Annu. Rev. Cell Dev. Biol 13, 83–117 (1997). [PubMed: 9442869]
4. Brouhard GJ & Rice LM Microtubule dynamics: an interplay of biochemistry and mechanics. Nat. Rev. Mol. Cell Biol 19, 451–463 (2018). [PubMed: 29674711]
5. Song Y & Brady ST Post-translational modifications of tubulin: pathways to functional diversity of microtubules. Trends Cell Biol. 25, 125–136 (2015). [PubMed: 25468068]
6. Gadadhar S, Bodakuntla S, Natarajan K & Janke C The tubulin code at a glance. J. Cell Sci 130, 1347–1353 (2017). [PubMed: 28325758]
7. Magiera MM, Singh P, Gadadhar S & Janke C Tubulin Posttranslational Modifications and Emerging Links to Human Disease. Cell 173, 1323–1327 (2018). [PubMed: 29856952]
8. Magiera MM, Singh P & Janke C SnapShot: Functions of Tubulin Posttranslational Modifications. Cell 173, 1552–1552 e1 (2018). [PubMed: 29856960]
9. Nieuwenhuis J & Brummelkamp TR The Tubulin Detyrosination Cycle: Function and Enzymes. Trends Cell Biol. 29, 80–92 (2019). [PubMed: 30213517]
10. Arce CA, Rodriguez JA, Barra HS & Caputo R Incorporation of L-tyrosine, L-phenylalanine and L-3,4-dihydroxyphenylalanine as single units into rat brain tubulin. Eur. J. Biochem 59, 145–149 (1975). [PubMed: 1204603]
11. Raybin D & Flavin M An enzyme tyrosylating alpha-tubulin and its role in microtubule assembly. Biochem. Biophys. Res. Commun 65, 1088–1095 (1975). [PubMed: 1156416]
12. Hallak ME, Rodriguez JA, Barra HS & Caputto R Release of tyrosine from tyrosinated tubulin. Some common factors that affect this process and the assembly of tubulin. FEBS Lett. 73, 147–150 (1977). [PubMed: 838053]
13. Ersfeld K et al. Characterization of the tubulin-tyrosine ligase. J. Cell Biol 120, 725–732 (1993). [PubMed: 8093886]
14. Szyk A, Deaconescu AM, Piszczek G & Roll-Mecak A Tubulin tyrosine ligase structure reveals adaptation of an ancient fold to bind and modify tubulin. Nat. Struct. Mol. Biol 18, 1250–1258 (2011). [PubMed: 22020298]
15. Arce CA & Barra HS Release of C-terminal tyrosine from tubulin and microtubules at steady state. Biochem J. 226, 311–317 (1985). [PubMed: 3977875]
16. Gundersen GG, Khawaja S & Bulinski JC Postpolymerization detyrosination of alpha-tubulin: a mechanism for subcellular differentiation of microtubules. J. Cell Biol 105, 251–264 (1987). [PubMed: 2886509]
17. Steinmetz MO & Akhmanova A Capturing protein tails by CAP-Gly domains. Trends Biochem. Sci 33, 535–545 (2008). [PubMed: 18835717]
18. Erck C et al. A vital role of tubulin-tyrosine-ligase for neuronal organization. Proc. Natl. Acad. Sci. U. S. A 102, 7853–7858 (2005). [PubMed: 15899979]
19. Kerr JP et al. Detyrosinated microtubules modulate mechanotransduction in heart and skeletal muscle. Nat. Commun 6, 8526 (2015). [PubMed: 26446751]
20. Robison P et al. Detyrosinated microtubules buckle and bear load in contracting cardiomyocytes. Science 352, aaf0659 (2016). [PubMed: 27102488]
21. Barisic M et al. Mitosis. Microtubule detyrosination guides chromosomes during mitosis. Science 348, 799–803 (2015). [PubMed: 25908662]
22. Aillaud C et al. Vasohibins/SVBP are tubulin carboxypeptidases (TCPs) that regulate neuron differentiation. Science 358, 1448–1453 (2017). [PubMed: 29146868]
23. Nieuwenhuis J et al. Vasohibins encode tubulin detyrosinating activity. Science 358, 1453–1456 (2017). [PubMed: 29146869]
24. Iqbal Z et al. Loss of function of SVBP leads to autosomal recessive intellectual disability, microcephaly, ataxia, and hypotonia. Genet. Med doi: 10.1038/s41436-018-0415-8 (2019).
25. Fonrose X et al. Parthenolide inhibits tubulin carboxypeptidase activity. Cancer Res. 67, 3371–3378 (2007). [PubMed: 17409447]

26. Chatterjee D, Boyd CD, O'Toole GA & Sondermann H Structural characterization of a conserved, calcium-dependent periplasmic protease from Legionella pneumophila. J. Bacteriol 194, 4415–4425 (2012). [PubMed: 22707706]

27. Sanchez-Pulido L & Ponting CP Vasohibins: new transglutaminase-like cysteine proteases possessing a non-canonical Cys-His-Ser catalytic triad. Bioinformatics 32, 1441–1445 (2016). [PubMed: 26794318]

28. Lopez-Franco O et al. Parthenolide modulates the NF-kappaB-mediated inflammatory responses in experimental atherosclerosis. Arterioscler. Thromb. Vasc. Biol 26, 1864–1870 (2006). [PubMed: 16741149]

29. Guzman ML et al. The sesquiterpene lactone parthenolide induces apoptosis of human acute myelogenous leukemia stem and progenitor cells. Blood 105, 4163–4169 (2005). [PubMed: 15687234]

30. Duan D, Zhang J, Yao J, Liu Y & Fang J Targeting Thioredoxin Reductase by Parthenolide Contributes to Inducing Apoptosis of HeLa Cells. J. Biol. Chem 291, 10021–10031 (2016). [PubMed: 27002142]

Methods-only References

31. Minor W, Cymborowski M, Otwinowski Z & Chruszcz M HKL-3000: the integration of data reduction and structure solution--from diffraction images to an initial model in minutes. Acta Crystallogr. D Biol. Crystallogr 62, 859–866 (2006). [PubMed: 16855301]

32. Adams PD et al. PHENIX: a comprehensive Python-based system for macromolecular structure solution. Acta Crystallogr. D Biol. Crystallogr 66, 213–221 (2010). [PubMed: 20124702]

33. Emsley P & Cowtan K Coot: model-building tools for molecular graphics. Acta Crystallogr. D Biol. Crystallogr 60, 2126–2132 (2004). [PubMed: 15572765]

34. Emsley P, Lohkamp B, Scott WG & Cowtan K Features and development of Coot. Acta Crystallogr. D Biol. Crystallogr 66, 486–501 (2010). [PubMed: 20383002]

35. McCoy AJ Solving structures of protein complexes by molecular replacement with Phaser. Acta Crystallogr. D Biol. Crystallogr 63, 32–41 (2007). [PubMed: 17164524]

36. Chen VB et al. MolProbity: all-atom structure validation for macromolecular crystallography. Acta Crystallogr. D Biol. Crystallogr 66, 12–21 (2010). [PubMed: 20057044]

37. Ti SC et al. Mutations in Human Tubulin Proximal to the Kinesin-Binding Site Alter Dynamic Instability at Microtubule Plus- and Minus-Ends. Dev. Cell 37, 72–84 (2016). [PubMed: 27046833]

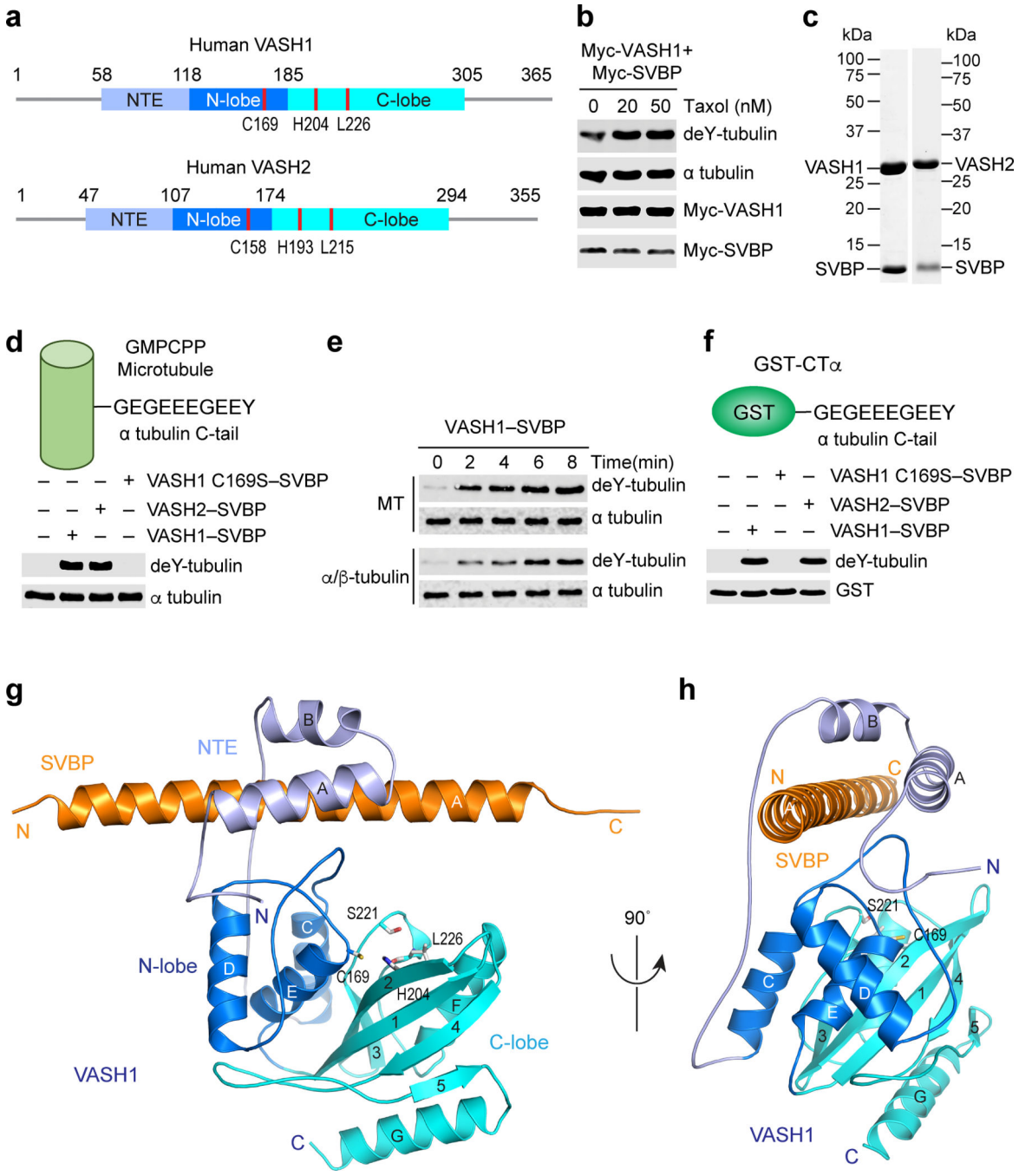

Fig. 1 |. Overall structure of the human VASH1–SVBP complex.

a, Domain diagram of human VASH1 and VASH2, with the catalytic triad indicated as red lines. The domain boundaries are indicated. NTE, N-terminal extension. **b**, Tubulin detyrosination assays of VASH1–SVBP in human cells. Lysates of HeLa Tet-On cells transfected with the indicated plasmids and treated without or with Taxol were blotted with the indicated antibodies. deY-tubulin, detyrosinated α tubulin. Experiments were repeated three times with similar results. **c**, Coomassie stained gel of purified recombinant human VASH1–SVBP and VASH2–SVBP complexes. **d-f**, *In vitro* detyrosination of GMPCPP-

stabilized human microtubules (MTs) (**d**,**e**), α–β tubulin heterodimer (**e**, bottom panels), or the C-terminal peptide of α tubulin (CTα) fused to GST (**f**) by the indicated recombinant VASH1–SVBP and VASH2–SVBP complexes. deY-tubulin, detyrosinated α tubulin. Experiments were repeated at least three times with similar results. **g**,**h**, Ribbon diagram of the crystal structure of the $VASH1_{52–310}$–SVBP complex in two different views, with the catalytic triad and S221 shown as sticks. The secondary structural elements, N- and C-termini are labeled. The color scheme of VASH1 match that in **a**, with the NTE, N-lobe, and C-lobe colored in light blue, blue, and cyan, respectively. SVBP is colored orange. The same color scheme is used in all subsequent figures. All structure figures were generated with PyMOL (http://www.pymol.org/). Uncropped gel and blot images of **b-f** are included in Supplementary Data Set 1.

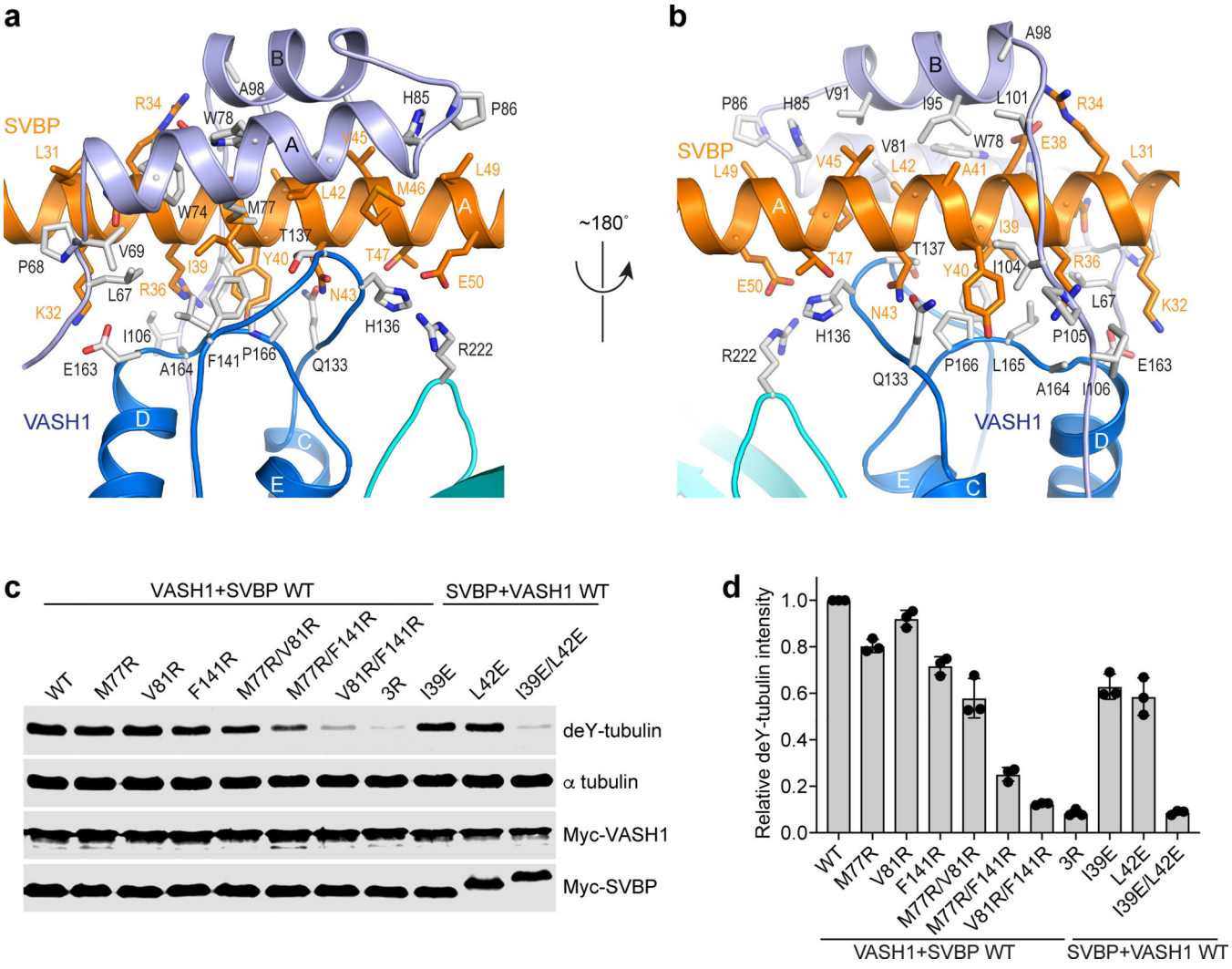

Fig. 2 |. The VASH1–SVBP interface.

a,**b**, Close-up views of the VASH1–SVBP interface, with interacting residues shown as sticks. VASH1 residues are colored gray and labeled with black letters while SVBP residues are colored orange and labeled with orange letters. The helices are labeled. **c**, Tubulin detyrosination assays of VASH1–SVBP in human cells. Lysates of HeLa Tet-On cells transfected with the indicated plasmids were blotted with the indicated antibodies. WT, wild-type; deY-tubulin, detyrosinated α tubulin. For unknown reasons, Myc-SVBP L42E and I39E/L42E mutants migrated with slower gel mobility. Uncropped blot images are included in Supplementary Data Set 1. **d**, Quantification of the relative detyrosination levels of α tubulin in **c** (mean ± SD, n = 3 independent experiments). Source data for **d** are available in Supplementary Data Set 2.

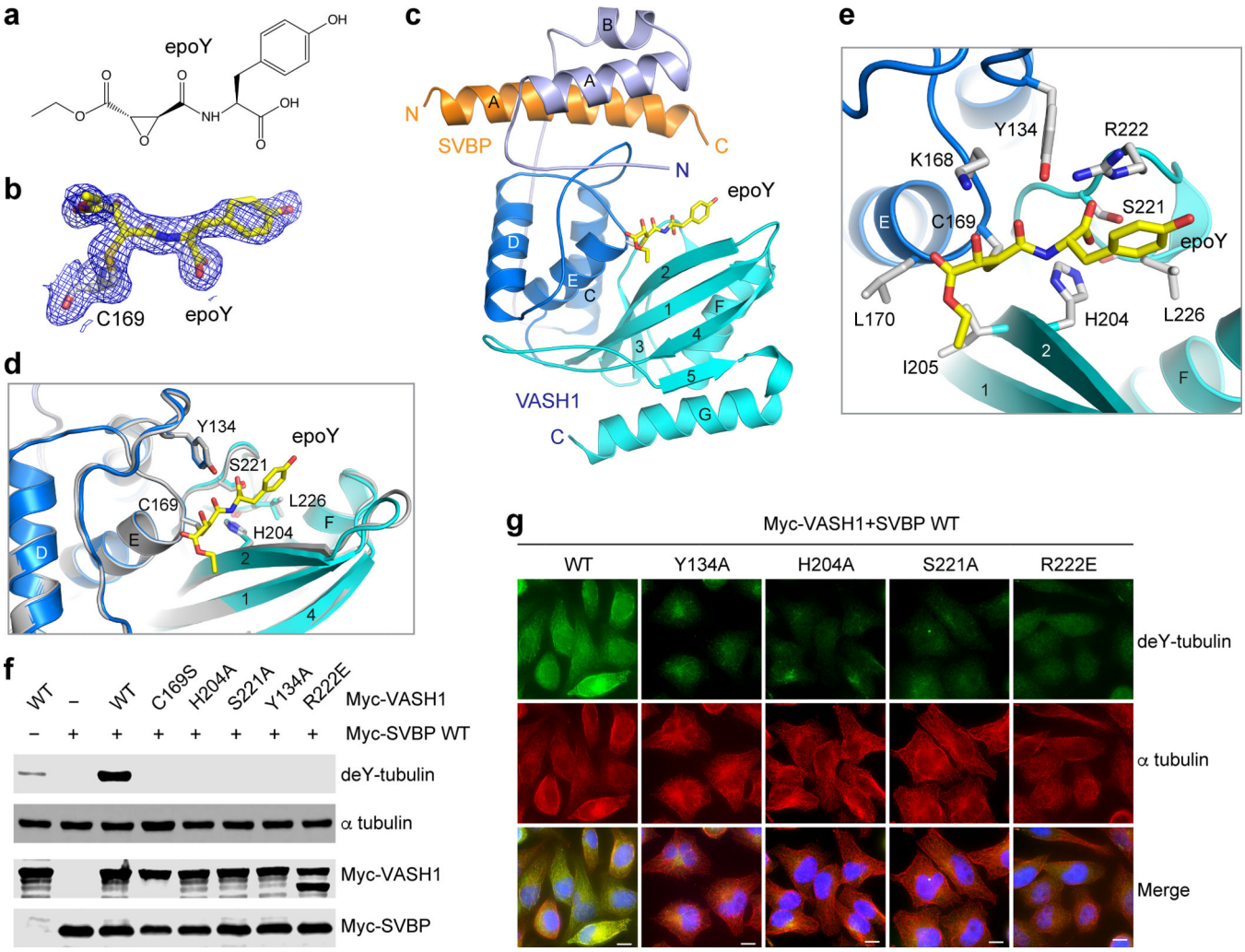

Fig. 3 |. Recognition of the C-terminal tyrosine by VASH1.

a, Chemical structure of epoY. **b**, The 2Fo-Fc composite omit map of epoY covalently attached to VASH1 C169 (contoured at 1.0 σ, carve=1.8Å). **c**, Ribbon diagram of the crystal structure of the VASH1–SVBP–epoY complex, with epoY and C169 shown as sticks. **d**, Superimposition of the apo-VASH1–SVBP (blue and cyan ribbon) and epoY-bound VASH1–SVBP (gray ribbon). **e**, Close-up view of the interactions between VASH1 and epoY. **f**, Tubulin detyrosination assays of VASH1–SVBP in human cells. Lysates of HeLa Tet-On cells transfected with the indicated plasmids were blotted with the indicated antibodies. WT, wild-type; deY-tubulin, detyrosinated α tubulin. Uncropped blot images are included in Supplementary Data Set 1. Experiments were repeated three times with similar results. **g**, HeLa Tet-On cells were co-transfected with Myc-SVBP WT and the indicated VASH1 WT or mutant plasmids and stained with anti-α tubulin (red) and detyrosinated tubulin (deY-tubulin) (green) antibodies and DAPI (blue). Scale bars, 10 μm. Experiments were repeated three times with similar results.

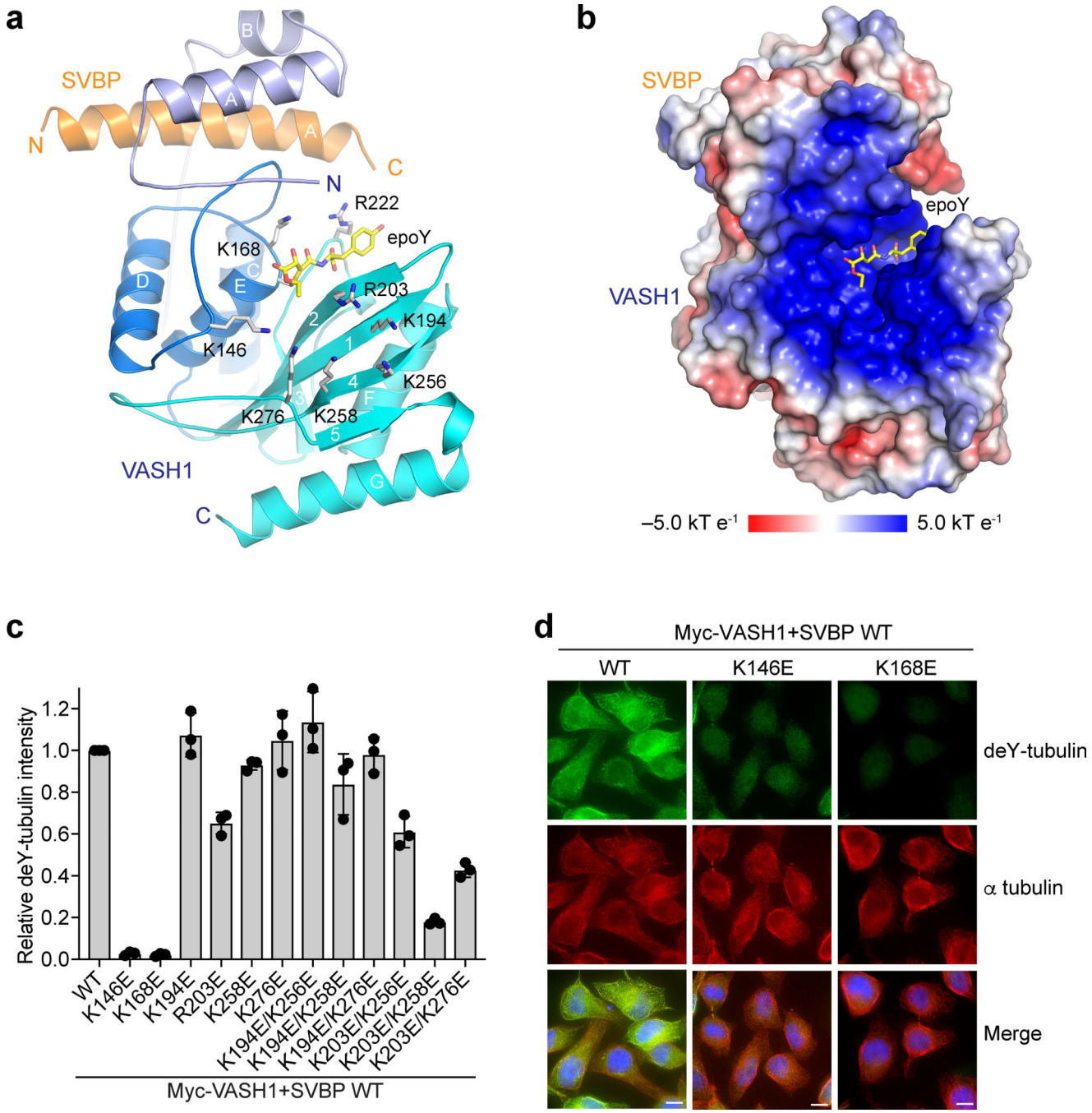

Fig. 4 |. Requirement for basic residues lining the substrate-binding cleft in tubulin detyrosination.

a, Ribbon diagram of the VASH1–SVBP–epoY complex with epoY and several basic residues that line the substrate-binding cleft shown as yellow and gray sticks, respectively. **b**, Solvent accessible surface of the VASH1–SVBP–epoY complex colored by electrostatic potential (blue, positive; red, negative). epoY is shown as sticks. **c**, Quantification of the relative detyrosination activities of the indicated VASH1 mutants in human cells as determined by immunoblotting (mean ± SD, n = 3 independent experiments). Representative

immunoblots are shown in Supplementary Fig. 4. Source data for **c** are available in Supplementary Data Set 2. **d**, HeLa Tet-On cells were co-transfected with Myc-SVBP WT and the indicated VASH1 WT or mutant plasmids and stained with anti-α tubulin (red) and detyrosinated tubulin (deY-tubulin) (green) antibodies and DAPI (blue). Scale bars, 10 μm.

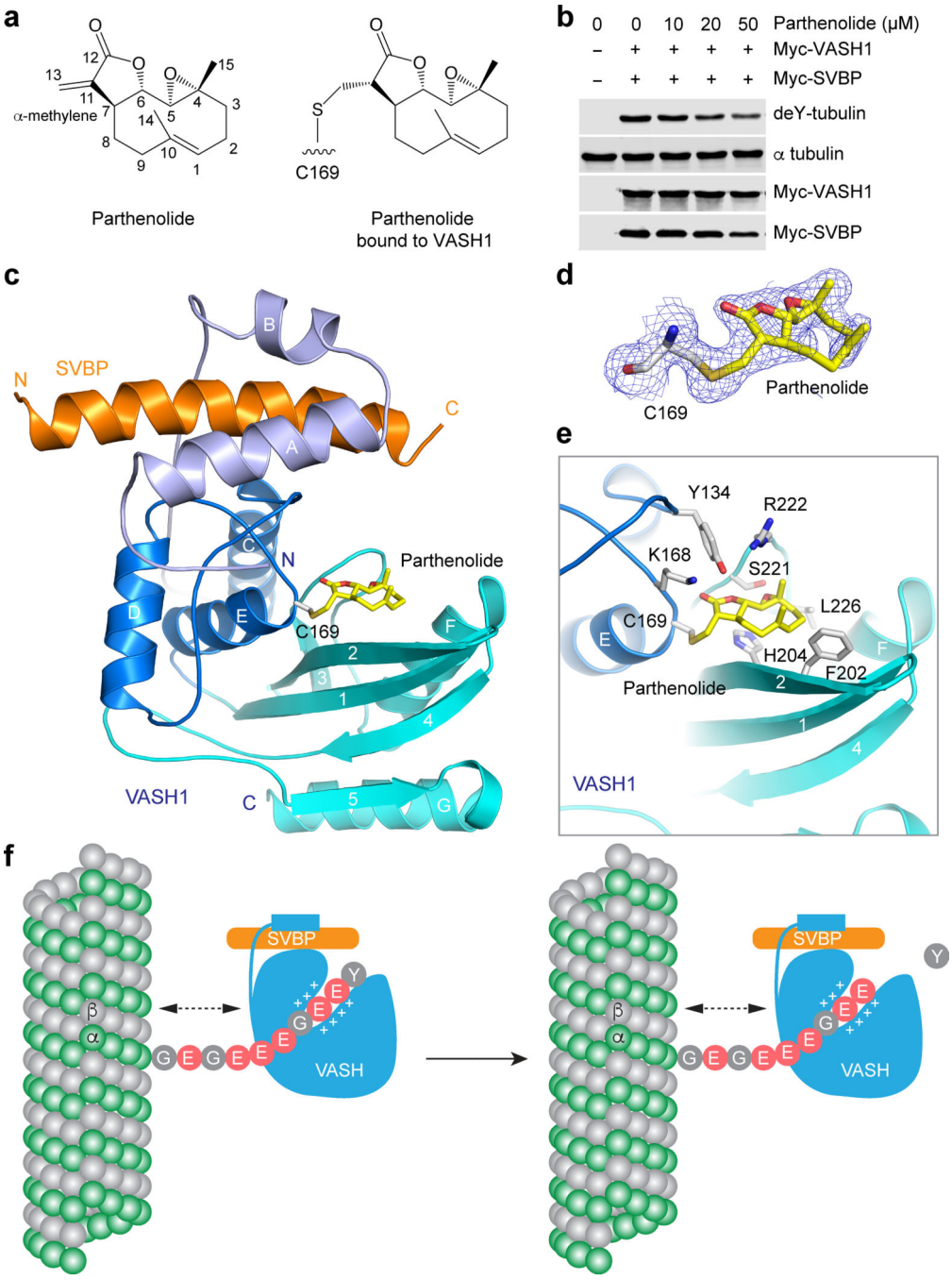

Fig. 5 |. Mechanism of VASH1 inhibition by parthenolide.

a, Chemical structures of parthenolide before and after its covalent attachment to VASH1 C169. **b**, Inhibition of VASH1–SVBP-dependent tubulin detyrosination by parthenolide. HeLa Tet-On cells were co-transfected with Myc-VASH1 and Myc-SVBP plasmids and treated with increasing doses of parthenolide for 8 hours. Cell lysates were blotted with the indicated antibodies. deY-tubulin, detyrosinated α tubulin. Uncropped blot images are included in Supplementary Data Set 1. Experiments were repeated three times with similar results. **c**, Ribbon diagram of the crystal structure of the VASH1–SVBP–parthenolide

complex, with parthenolide and C169 shown as sticks. **d**, The 2Fo-Fc composite omit map of parthenolide covalently linked to C169 (contoured at 1.0 σ, carve=1.8Å). **e**, Close-up view of the interactions between VASH1 and parthenolide. **f**, Model of substrate recognition and tubulin detyrosination by VASH1–SVBP and VASH2–SVBP. The "+"s indicate positive charges. The dashed line indicates unidentified interactions between VASH–SVBP and the microtubule lattice.

Table 1 |

Data collection, phasing and refinement statistics

	SeMet VASH1–SVBP (6OCF)	VASH1–SVBP–epoY (6OCG)	VASH1–SVBP–parthenolide (6OCH)
Data collection			
Space group	$I4_122$	$P2_12_12$	$P2_12_12_1$
Cell dimensions			
a, *b*, *c* (Å)	100.56, 100.56, 206.73	70.67, 126.45, 46.08	70.13, 90.16, 127.24
α, *β*, *γ* (°)	90, 90, 90	90, 90, 90	90, 90, 90
Wavelength	0.9792	0.9792	0.9792
Resolution (Å)	50.00–2.10 (2.14–2.10)[a]	50.00–1.83 (1.86–1.83)	50.00–2.00 (2.03–2.00)
R_{merge}	0.088 (2.568)	0.056 (3.541)	0.150 (2.046)
$I/\sigma(I)$	42.8 (1.1)	50.2 (1.4)	19.3 (1.6)
$CC_{1/2}$	99.9 (54.7)	99.8 (61.7)	99.8 (54.5)
Completeness (%)	99.6 (97.0)	99.6 (99.8)	99.9 (100.0)
Redundancy	24.5 (20.4)	13.1 (13.3)	13.0 (12.8)
Refinement			
Resolution (Å)	45.21–2.10	46.08–1.83	47.12–2.00
No. reflections	25,607 (1,281 in test set)	33,221 (1,661 in test set)	52,632 (1,998 in test set)
R_{work} / R_{free}	0.196 / 0.222	0.177 / 0.217	0.180 / 0.228
No. atoms			
Protein	2,523	2,396	4,484
Ligand/ion	7[b]	30[c]	72[d]
Water	168	341	561
B factors			
Protein	41.77	28.40	32.64
Ligand/ion	37.15	47.06	66.41
Water	44.98	39.40	41.03
R.m.s deviations			
Bond lengths (Å)	0.007	0.007	0.007
Bond angles (°)	0.897	0.823	0.843

One crystal was used for each structure.

[a]Values in parentheses are for highest-resolution shell.

[b]Bound ligands include one glycerol and one chloride ion.

[c]Bound ligands include one glycerol, one chloride ion, and one epoY molecules.

[d]Bound ligands include one glycerol, six sulfate ions, and two parthenolide molecules.

Table 2 |

Catalytic activities of VASH1 wild-type (WT) and mutants

VASH1	k_{cat} (min^{-1})	K_m (μM)	k_{cat} K_m^{-1} (μM^{-1} min^{-1})
WT	44.5	7.9	5.6
H204A	3.4	8.9	0.38
S221A	15.5	360.7	0.043
Y134A	4.1	280.1	0.015
K146E	13.3	515.2	0.026
K168E	15.7	366.7	0.043

Source data for this table are available in Supplementary Data Set 2.